Journal of Electroceramics, 8, 49–55, 2002

Electrochemical Gas Sensor Materials Studied by Impedance Spectroscopy Part I: Nasicon as a Solid Electrolyte

P. PASIERB,* S. KOMORNICKI, R. GAJERSKI & S. KOZIŃSKI
Faculty of Materials Science and Ceramics, University of Mining and Metallurgy, 30-059 Cracow, Poland

P. TOMCZYK
Faculty of Fuels and Energy, University of Mining and Metallurgy, 30-059 Cracow, Poland

M. RĘKAS
School of Materials Science and Engineering, The University of New South Wales, UNSW Sydney, NSW 2052, Australia

Submitted August 6, 2001; Revised February 27, 2002; Accepted March 12, 2002

Abstract. Impedance spectra of the solid electrolyte (Nasicon) were investigated by means of complex impedance in the frequency range 0.1 Hz–1 MHz at temperatures between 298 and 873 K. A plausible equivalent circuit consisting of resistor and constant phase element in series was proposed. Pronounced effect of electrode structure on impedance spectra has been observed. The equivalent circuit for the sample with Pt blocking electrodes in the temperature range 298 K–773 K is composed mostly of the CPE element, representing electrode-material interface (Warburg impedance). On the other hand, the Nasicon sample with porous Pt electrodes may be simulated by the circuit formed from the resistance R and the CPE element in series. At 573 K and above the CPE element is reduced to the simple Debye capacitor. The determined electrical conductivity and activation energy of conductivity are in general agreement with those for bulk of Nasicon reported in the literature.

Keywords: impedance spectroscopy, electrochemical gas sensors, solid electrolytes, Nasicon

1. Introduction

The Nasicon, $Na_{1+x}Zr_2Si_xP_{3-x}O_{12}$ (with $1 \leq x \leq 3$), has been proposed by Hong et al. [1, 2] for many electrochemical devices such as batteries, ion selective membranes and electrochemical sensors. It is one of the best Na^+ ion conducting solid electrolytes. It consists of ZrO_6 octahedrons linked by corners to $(Si, P)O_4$ tetrahedra [2]. Sodium ions are located in three-dimensional lattice channels. The conductivity mechanism of Na^+ containing Nasicon is similar to that of β-aluminas. However, contrary to β-alumina, Nasicon is less sensitive to degradation by moisture [3].

*To whom all correspondence should be addressed.

Taking into account the properties mentioned above, this ionic conductor seems to be the most promising solid electrolyte for constructing an electrochemical gas sensors. Many types of electrochemical sensors that employ Nasicon as a solid electrolyte have been tested for monitoring CO_2, SO_x and NO_x gases [4–12], but no respectable characteristics for practical use has been achieved so far. The main disadvantage of many proposed sensors is a long-time instability of the sensor signal. The elucidation of processes occurring in the sensor is essential for the improvement of the sensor characteristics.

The purpose of our study, reported in the present and the following paper [13], is to find the mechanism of charge transfer inside the solid electrochemical cells

used as gas sensors. This understanding is fundamental for processing of both solid electrolyte and electrode materials with controlled properties for high performance and reliable electrochemical gas sensors. This paper presents the obtained data of the charge transfer in the solid electrolyte (Nasicon) determined on the basis of the impedance spectroscopy measurements. The observed electrical properties and effects are discussed from the points of view of electrode, bulk and interface properties.

2. Experimental Details

2.1. Solid Electrolyte Preparation

The $Na_3Zr_2Si_2PO_{12}$ (Nasicon) samples were prepared by a solid-state reaction method. The appropriate amounts of $ZrSiO_4$ and $Na_3PO_4 \cdot 12\,H_2O$ powders (ACS grade 99+%, Sigma-Aldrich) were crushed and mixed in a vibrational mill with ZrO_2 balls in ethyl alcohol suspension to form a fine powder mixture. After drying at 373 K the powder was pressed in a pellet die and the samples obtained were calcined at 1373 K for 48 hours. The pellets were again crushed in an agate mortar, once more milled, uniaxially pressed into pellets at 70 MPa, isostatically pressed at 200 MPa, then sintered at 1523 K for 20 hours. Subsequently, the sintered pellets were polished using diamond paste to the approx. diameter of 10.7 mm and thickness of 1.8 mm, cleaned in alcohol using an ultrasonic cleaner, dried at 373 K and stored in a desiccator until used for preparation of samples or further experiments.

The X-ray diffraction measurements have shown that the material has the structure of monoclinic $Na_3Zr_2Si_2PO_{12}$ with a very slight admixture of ZrO_2 phase. The measured density of the samples was about 95% of the theoretical density (3.16 g/cm^3).

2.2. Electrode Formation

Two types of platinum electrodes were applied at the both sides of Nasicon pellets for the impedance measurements:

(1) platinum solid plates (sample labelled as "*N1*"), or
(2) porous platinum electrodes prepared by screen printing method (sample labelled as "*N2*").

The porous platinum electrodes at the Nasicon pellets were fabricated by subsequent screen printing of platinum paste (prod. Demetron, Germany), then dried at the room temperature and fired at 1173 K for 30 minutes.

2.3. Impedance Measurements

The impedance measurements were performed using an IM5d Impedance Spectrum Analyser (Zahner Elektrik) in the frequency range 0.1 Hz–1 MHz. The amplitude of sinusoidal voltage signal was 20 mV. All the measurements were carried out in air in the temperature range 298–873 K. Prior to any measurement each sample was kept for at least 30 minutes at the experimental conditions (after temperature change) in order to allow the sample to reach the equilibrium.

3. Results

Figures 1–5 illustrate typical experimental results for the samples *N1* and *N2* presented in either complex impedance (Figs. 1–3) or complex admittance coordinates (Figs. 4 and 5). The dependences of Z'' on Z' can be estimated by one (Figs. 2 and 3) or two straight lines (Fig. 1). At the lower temperatures (298 K and 573 K) the plots cross the initial point of the coordinates (0, 0). At the higher temperatures (623 K and above) the intersects of the plots with Z' axes are positive.

On the other hand, in the case of the sample *N2* at 573 K and higher temperatures the admittance plots may be approximated by circles (Fig. 5). The centers of the circles are located below of the Y' axis. Only at the room temperature the admittance plot for the sample *N2* has a different shape, as presented in Fig. 4.

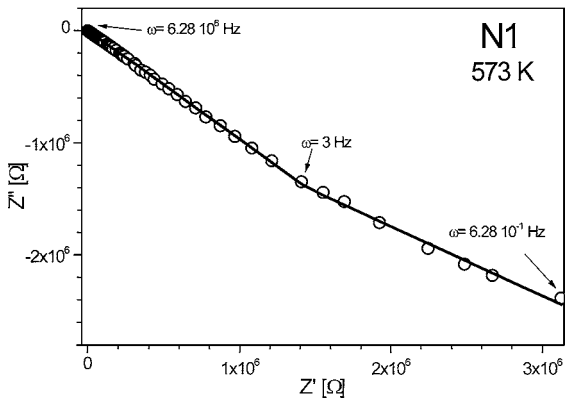

Fig. 1. Plot Z'' vs. Z' for the sample *N1* at 573 K.

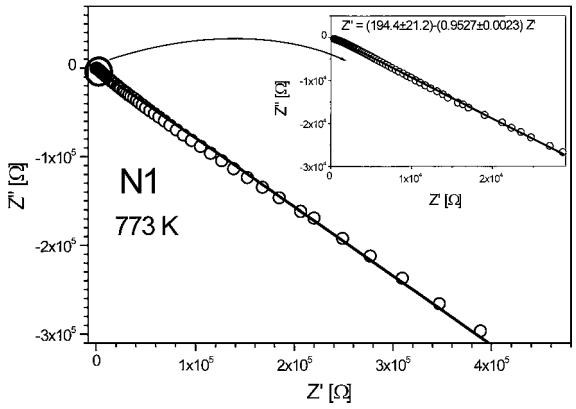

Fig. 2. Plot Z'' vs. Z' for the sample *N1* at 773 K. Inset illustrates the enlarged segment at the high frequencies.

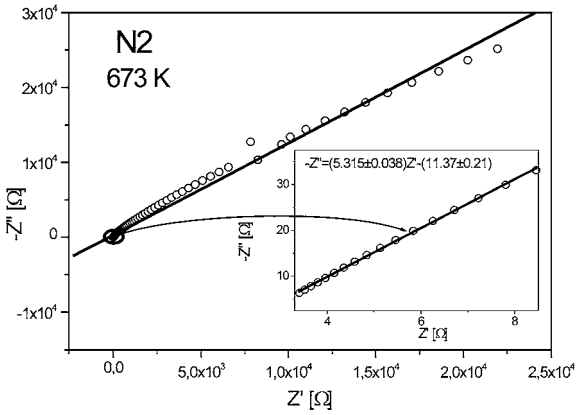

Fig. 3. Plot Z'' vs. Z' for the sample *N2* at 673 K. Inset illustrates the enlarged segment at the high frequencies.

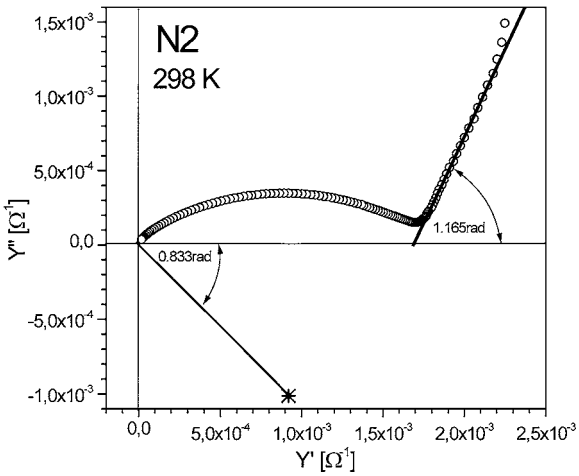

Fig. 4. Plot Y'' vs. Y' for the sample *N2* at 298 K.

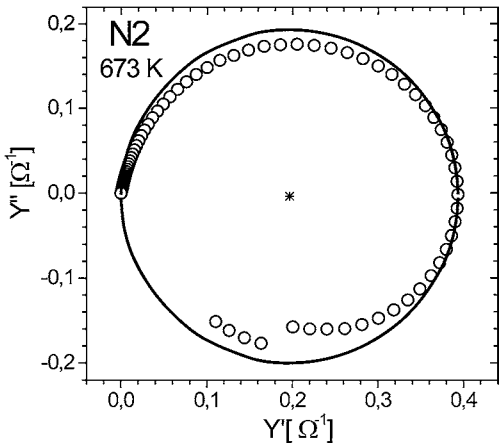

Fig. 5. Plot Y'' vs. Y' for the sample *N2* at 673 K.

4. Discussion

4.1. Analysis of Equivalent Circuits

In order to explain the observed dependencies we have analysed several equivalent circuits consisting of a set of resistors, capacitors and inductances with constant parameters (so called Debye elements) or non-Debye elements such as a *C*onstant *P*hase *E*lement, CPE [14]. The impedance behavior of the equivalent circuit has to be identical with the behavior found for the sample. Moreover, the elements proposed in the equivalent circuit must have a physical meaning.

The circuit proposed in Fig. 6(a) is the most simplest equivalent circuit that approximated the impedance of the studied samples with a good accuracy. The impedance of the CPE element, Z_{CPE} is defined by [14]

$$Z_{\mathrm{CPE}} = A(j\omega)^{-\frac{1}{n}} \tag{1}$$

where A and n are constants, j is the imaginary unit and ω is an angular frequency. In particular, for $n = 2$ the CPE element is termed a Warburg impedance, while for $n = 1$ the CPE is reduced to the Debye capacitor with capacitance $1/A$ and, finally for the parameter n approaching the infinity the element CPE represents a resistor with resistance A.

Considering the equivalent circuit composed of a resistance R and a CPE element connected in series, as shown in Fig. 6(a), we obtain for the impedance

$$Z = Z' + jZ'' = R + Z_{\mathrm{CPE}} = R + A(j\omega)^{-\frac{1}{n}} \tag{2}$$

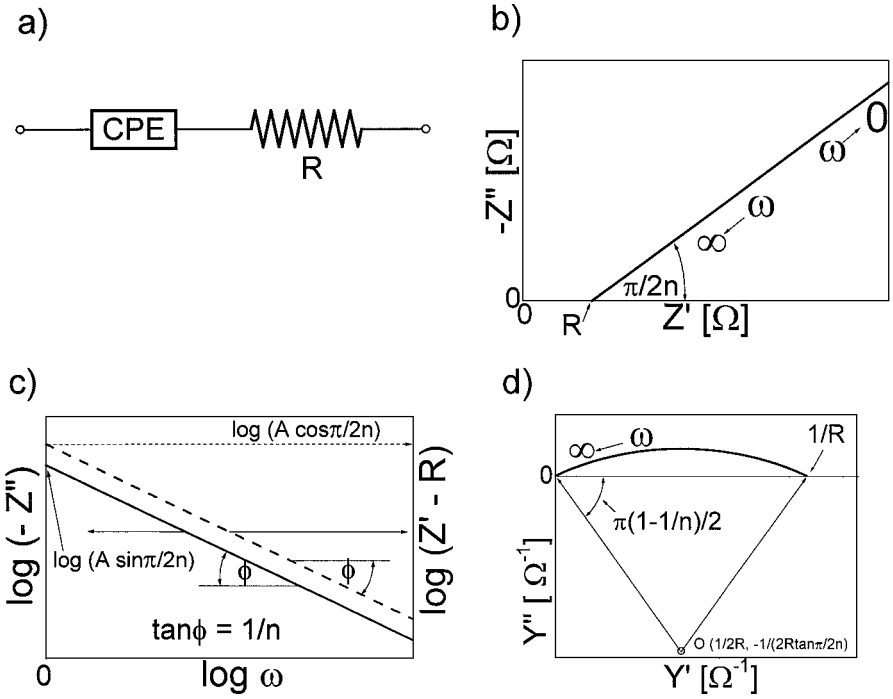

Fig. 6. Equivalent circuits (a) and schematically plots of dependencies: $-Z''$ vs. Z' (b), $\log(-Z'')$ vs. $\log\omega$ (c), Y'' vs. Y' (d).

From Eq. (2) we get the real and imaginary part of the impedance

$$Z' = R + A\omega^{-\frac{1}{n}} \cos\frac{\pi}{2n} \tag{3}$$

and

$$-Z'' = A\omega^{-\frac{1}{n}} \sin\frac{\pi}{2n} \tag{4}$$

Combining Eqs. (3) and (4) results in

$$-Z'' = (Z' - R)\tan\frac{\pi}{2n} \tag{5}$$

According to Eq. (5) we are able to determine both the parameters n and R from the slope of linear dependence of $(-Z'') = f(Z')$ and from the intersection of the straight line with Z' axis (Fig. 6(b)). Moreover, Eqs. (3) or (4) may also be used independently to determine the parameter n. Figure 6(b) and (c) illustrates schematically the dependencies (3)–(5) for arbitrarily chosen n, R and A. Fig. 6(d) illustrates the admittance plot corresponding to the considered circuit.

4.2. Sample N1 (Nasicon with Pt-Plate Electrodes)

Figure 7 illustrates an example of the dependencies given by Eqs. (3) and (4) obtained for the sample *N1* at 573 K. The performed error estimation analysis indicates that the n parameter values can be determined from Eqs. (3) or (4) more precisely than from Eq. (5). Figure 8 shows the dependences of parameter n obtained from Eqs. (3)–(5) on the temperature. According to Fig. 8 in the temperature range 573 K–873 K the parameter n assumes values close to 2, corresponding to the Warburg impedance.

In the lower temperature range, up to 573 K (Fig. 1), the plot can be approximated by two straight lines with the interesection at the point (0, 0). In this temperature range the total impedance is mostly controlled by the component Z_{CPE}, rather than R. The absence of the other elements in the equivalent circuit may be explained by the predominance of the Warburg impedance [14] in this case.

For the higher temperatures, 623 K and above only one straight line is observed and the intersection with Z'' axis yields positive values. Hence, the parameter n can be determined from the slope and

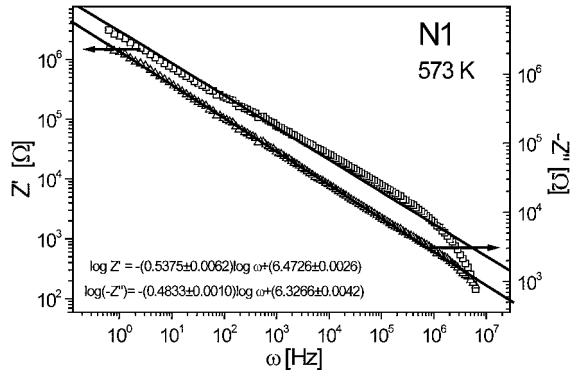

Fig. 7. Dependencies of Z' and $(-Z'')$ vs. angular frequency for the sample *N1* at 573 K.

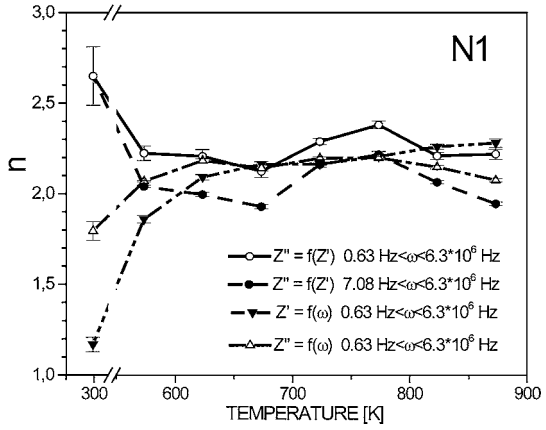

Fig. 8. Parameter of n for *N1* as a function of temperature, determined from the following dependencies: $Z'' = f(Z')$, $Z' = f(\omega)$ and $Z'' = f(\omega)$.

R from the intercept of the linear dependence (see Fig. 2).

4.3. *Sample N2 (Nasicon with Porous Pt-Film Electrodes)*

The replacement of Pt plates by porous Pt layers results in the reduction of CPE participation in the total impedance within the whole temperature range. In this case we are able to determine the resistance R and CPE components from the complex plots of impedances and admittances. Typical experimental results obtained for the sample *N2* at room temperature are presented in Fig. 4 (in the coordinates Y'' vs. Y'). The experimental points may be approximated by the *arc*-part of the semicircle and the '*spur*'. Similar relations have been observed for CdF_2 at 336 K [15], for β-alumina at 169 K [16]. These results may be described by the circuit presented in Fig. 6(a) modified by addition of a second CPE element parallel to the resistor R. Such circuits were analysed by Bauerle [17] for the ideal case, where both the CPE elements were replaced by the Debye capacitors. Under this conditions the "*spur*" is perpendicular to the Y' axis. The angle between the "*spur*" and Y' axis in Fig. 4 is equal to 1.165 ± 0.003 rad ($66°45'$). This corresponds to the value of parameter n for the second CPE element $n_2 = 1.348 \pm 0.030$.

The typical impedance spectra of the sample *N2* obtained at higher temperatures (573 K and above) are illustrated in Figs. 3 and 5, in the complex impedance and admittance coordinates, respectively. For the positive values of Y'' the experimental points may be represented by a semicircle, crossing the Y' axis in the points $(0, 0)$ and $(1/R, 0)$. The fitted parameters of the sample *N2* in the complex admittance coordinates are shown in the Table 1. As can be seen, the parameter n_i assumes values close to 1 in the temperature range 573 K–873 K. It means, that the CPE element illustrated in Fig. 6(a) is reduced to the simple Debye capacitor. Moreover, at higher frequencies the experimental points represent negative values of Y'' (Fig. 5). The presence of such points indicates the inductance effects from the connecting wires.

Considering the *R-L-C* circuit represented by resistance R, inductance L and capacitance C connected in series, we shall get the following relationship:

$$\omega \tan\theta = -\frac{L}{R}\omega^2 + \frac{1}{RC} \tag{6}$$

where θ is the phase angle ($\tan = Z''/Z'$). Figure 9 illustrates the dependence $\omega \tan\theta$ vs. ω^2 for the sample

Table 1. Admittance analysis of the sample *N2* $(Y'-a)^2+(Y''-b)^2 = a^2+b^2$.

T (K)	a (Ω^{-1})	b (Ω^{-1})	n
298	0.0010	−0.0003	2.129
573	0.1328	−0.0017	1.008
623	0.1695	−0.0075	1.029
673	0.1897	−0.0036	1.012
723	0.2130	−0.0029	1.009
773	0.2264	−0.0053	1.015
823	0.2339	−0.0134	1.038
873	0.2368	−0.0272	1.079

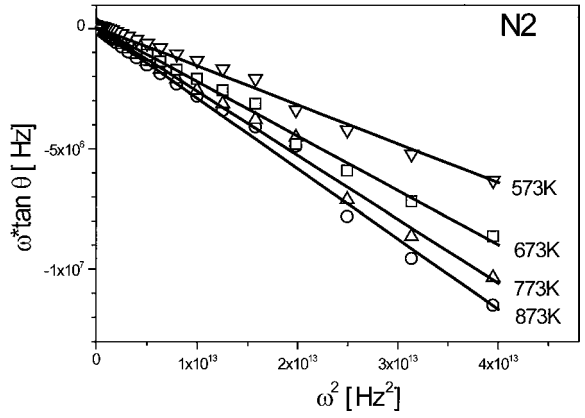

Fig. 9. Dependence $\omega \tan\theta$ vs. ω^2 for the sample *N2* at 573–873 K.

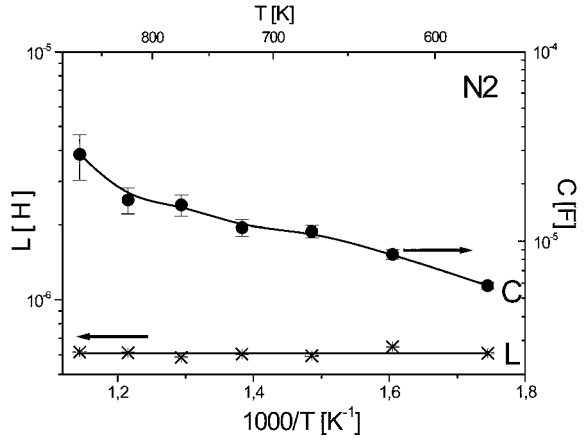

Fig. 10. Inductance L and capacitance C as a function of reciprocal temperature for the sample *N2*.

N2 at various temperatures. The data from Table 1 and the parameters of the straight line from Fig. 9 allow us to determine both L and C. Figure 10 illustrates the temperature dependences of L and C. The capacitance values are of the order 10^{-5}–10^{-6} F and increase with temperature. On the other hand, the inductance L is independent of temperature and equal to 0.609 ± 0.019 μH. This value is typical for the inductance of lead connections.

4.4. The Temperature Dependence of Resistivity

The dependencies of $\log(\sigma T)$ vs. 1/T for *N1* and *N2* samples are presented in Fig. 11. The sample *N2* shows an electrical conductivity that is several times higher

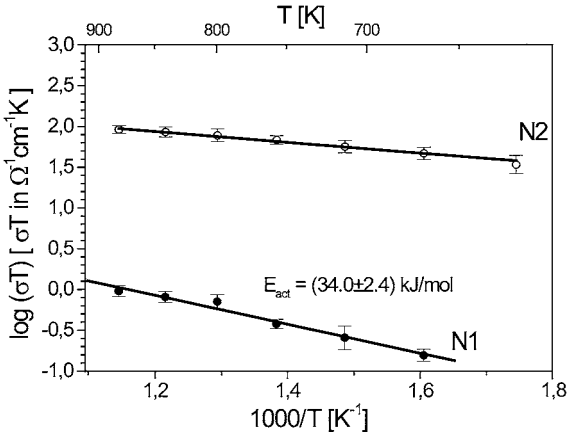

Fig. 11. Plot $\log(\sigma T)$ vs. $1/T$ for the samples *N1* and *N2*.

than that of the *N1* sample. Table 2 reports the literature data for the electrical conductivity at 573 K and activation energy of Nasicon [2, 18–25] in comparison with the data obtained in this work. The determined values of the electrical conductivity and the activation energy of the sample *N2* are similar to those reported in the literature. Much lower electrical conductivity of the

Table 2. Electrical conductivity and activation energy for $Na_{1+x}Zr_2P_{3-x}Si_xO_{12}$ (Nasicon).

x	$\sigma_{573\ K}$ ($\Omega^{-1}cm^{-1}$)	E_{act} (kJ/mol)	References
1.2	0.026	26.1	
1.8	0.125	23.2	
2.0	0.20	28.0	[2]
2.2	0.17	23.2	
2.8	0.018	23.2	
2.0	0,17	20	[19]
1.6	0.14	20.3	
1.8	0.11	22.2	
2.0	0.093	19.3	[20]
2.2	0.12	19.3	
2.4	0.061	28.9	
2.0		20.0–20.3	[21]
2.2		15.8	[22]
2.32		19.5	
1.8	0.089–0.257	17.4–28.0	[23]
2.0	0.11–0.285	17.4–25.1	
2.2	0.12–0.27	18.3	
1.2	0.0132	13.9	[24]
1.5	0.0282	15.5	
2.0	0.201	13.3	
2.0		22.6–38.1	[25]
2.0	0,082	31,8	[18]
2.0	0.063	13.7 ± 0.7	This work—sample *N2*
2.0	0.00016	34.0 ± 2.4	This work—sample *N1*

sample *N1* may be explained by poor electrical contacts between the electrodes and electrolyte.

5. Conclusions

The impedance spectra of the solid electrolyte (Nasicon) were investigated by analysis of the complex impedance spectra at the frequencies ranging from 0.1 Hz to 1 MHz and temperatures 298 K to 873 K. The distinct effect of the type of electrode on the impedance spectra was observed. The equivalent circuit for the sample with Pt blocking electrodes (*N1* sample) in the temperature range 298 K–773 K is composed mostly of the CPE element, representing electrode-material interface (Warburg impedance). On the other hand, the Nasicon sample with porous Pt electrodes (*N2* sample) may be simulated by the circuit formed from the resistance *R* and the CPE element in series. At 573 K and above the CPE element is reduced to the simple Debye capacitor. The determined electrical conductivity and activation energy of conductivity are in general agreement with those for bulk of Nasicon reported in the literature.

Acknowledgments

The financial support of Polish State Committee for Scientific Research (KBN), Project No. 7 T08A 037 15 is acknowledged.

References

1. H.Y.P. Hong, *Mater. Res. Bull*, **11**, 173 (1976).
2. J.B. Goodenough, H.Y.P. Hong, and J.A. Kafalas, *Mater. Res. Bull.*, **11**, 203 (1976).
3. J.J. Auborn and D.W. Johnson Jr., *Solid State Ionics*, **5**, 315 (1981).
4. K. Singh, P. Ambekar, and S.S. Bhoga, *Solid State Ionics*, **122**, 191 (1999).
5. Y.C. Zhang, H. Tagawa, S. Asakura, J. Mizusaki, and H. Narita, *J. Electrochem. Soc.*, **144**, 4345 (1997).
6. M. Holzinger, J. Maier, and W. Sitte, *Solid State Ionics*, **94**, 217 (1997).
7. D.J. Slater, R.V. Kumar, and D.J. Fray, *Solid State Ionics*, **86–88**, 1063 (1996).
8. T. Maruyama, Y. Saito, Y. Matsumoto, and Y. Yano, *Solid State Ionics*, **17**, 281 (1985).
9. S-D. Choi, W-Y. Chung, and D-D. Lee, *Sensors and Actuators*, **B 3536**, 263 (1996).
10. N. Miura, M. Ono, K. Shimanoe, and N. Yamazoe, *Sensors and Actuators*, **B 49**, 101 (1998).
11. Y. Shimizu and K. Maeda, *Sensors and Actuators*, **B 52**, 84 (1998).
12. N. Miura, M. Iio, G. Lu, and N. Yamazoe, *Sensors and Actuators*, **B 3536**, 124 (1996).
13. P. Pasierb, S.M. Komornicki, R. Gajerski, S. Kozinski, P. Tomczyk, and M. Rekas, *J. Electroceramics*, **8**, 57 (2002).
14. J.R. Macdonald and D.R. Franceschetti, in *Impedance Spectroscopy* edited by J.R. Macdonald (John Wiley & Sons, New York, 1987), p. 84.
15. F. Krok, W. Bogusz, and W. Jakubowski, *Phys. Stat. Sol.* (a), **60**, K65 (1980).
16. J.R. Dygas, G. Fafilek, and M.W. Breitner, *Solid State Ionics*, **119**, 115 (1999).
17. J.E. Bauerle, *J. Phys. Chem. Solids*, **30**, 2657 (1969).
18. O. Bohnke, S. Ronchetti, and D. Mazza, *Solid State Ionics*, **122**, 127 (1999).
19. U. von Alpen, M.F. Bell, and W. Wichelhaus, *Mat. Res. Bull.*, **14**, 1317 (1979).
20. J.P. Boilot, J.P. Salanie, G. Desplanches, and D. Le Potier, *Mat. Res. Bull.*, **14**, 1469 (1979).
21. W. Bogusz, *Phys. Stat. Sol.* (a), **66**, K109 (1981).
22. W. Bogusz, F. Krok, and W. Jakubowski, *Phys. stat. sol.* (a), **66**, K113 (1981).
23. A. Ahmad, T.A. Wheat, A.K. Kuriakose, J.D. Canaday, and A.G. McDonald, *Solid St. Ionics*, **24**, 89 (1987).
24. W. Bogusz, F. Krok, and W. Piszczatowski, *Solid St. Ionics*, **119**, 165 (1999).
25. J.R. Dygas, G. Fafilek, and M.W. Breiter, *Solid St. Ionics*, **119**, 115 (1999).